Design and Simulation Analysis of Robot-Assisted Plate Internal Fixation Device for Lower Limb Fractures

Yongqiang Zhou[1,2], Yimiao Chen[1,2], Chunsheng Sun[1,2] and Qinhe Zhang[1,2,*]

[1]*Key Laboratory of High Efficiency and Clean Mechanical Manufacture (Ministry of Education), School of Mechanical Engineering, Shandong University, Jinan 250061, China*

[2]*National Demonstration Center for Experimental Mechanical Engineering Education, Shandong University, Jinan 250061, China*

Abstract: Internal fixation with steel plates is a common method for the therapy of lower limb fractures. Due to the disadvantages of traditional surgical methods such as high trauma and complications, the application of robots for minimally invasive surgery has become a popular research direction. In this article, we have designed and simulated the overall structure of a steel plate internal fixation device used in conjunction with a robotic arm. Firstly, a finite element model of cortical bone drilling was established based on ABAQUS to obtain the torque and axial force when drilling the cortical bone. Then a virtual prototype of the robot-assisted lower limb bone fracture plate internal fixation device was designed, and the outer shell, drilling mechanism, nail placement mechanism, nail supply mechanism, drive mechanism, and guide sleeve were refined based on the overall mechanical structure of the device, so that the device could continuously perform drilling and nail placement. Afterward, the device was simulated based on ADAMS, and the motion curves of each component were obtained to verify the feasibility of the device's working principle and to validate the performance of the servo. Finally, the modal analysis of the device was carried out with the finite element software ABAQUS, and the modal parameters of the first six orders were obtained, which were compared with the operating frequencies of the motor and the servo to verify that the device is not easy to resonate during normal operation, and the static strength checks of the key components were carried out, and the stress and deformation clouds and upper limits of flexural values of the components were obtained, which proved that the structure has stability.

Keywords: Lower extremity fracture, Plate internal fixation, Robot-assisted, Structural design, Simulation analysis.

1. INTRODUCTION

The internal fixation technique, which began to be used in orthopedic clinical surgery in the early twentieth century, is a procedure in which broken bones are directly fixed by attaching them with screws, plates, and wires. The main advantage of internal fixation surgery is that it can provide reliable support for the affected limb [1]. However, incisional internal fixation surgery requires a complete incision of the fracture area, which severely disrupts the blood circulation in the fracture area. Minimally invasive internal fixation, on the other hand, suffers from poor visualization and low precision. Orthopedic surgery robots are favored by orthopedic surgeons because of their accuracy and speed, and with the development and advancement of computer technology, the use of robotic systems in orthopedic surgery is becoming more and more common. As early as 1995, Bouazza-Marouf [2] *et al*. designed a robotic system dedicated to the internal fixation of femoral fractures. Browbank [3] *et al*. developed a robotic system for assisting the internal fixation of hip fractures, which achieved the function of precise drilling under X-ray guidance. Füchtmeier [4] *et al*. appropriately modified the RX130 Stubli robot to enable it to be used for femoral stem fracture repositioning and fixation and used force feedback sensors to record forces and moments in three axes. Maeda [5] *et al*. developed a robot-assisted fracture repositioning and fixation system (FRAC-Robo) to assist in anatomical repositioning and internal fixation process to maintain the repositioned state. In 2014, Beijing Jishuitan Hospital [6] developed an active-passive integrated spine surgery robot RSSS to help surgeons determine the nail tract with the assistance of image navigation. Hu Lei [7] *et al*. also designed a biplane navigation robotic system for the distal strangulation of intramedullary nails. And the accuracy and safety of the system were tested by preliminary experiments. The Spine Assist/Renaissance developed by Mazor, Israel, and the ROSA Spine developed by Medtech Medical, France, can be used for screw placement in spinal surgery, and both are dual approved by the European CE and the US FDA [8, 9].

This study designs a plate fixation device for lower extremity fracture surgery. The device is used with a robotic arm to continuously and accurately place screws and realize the function of drilling before placing nails, which is of positive significance to improve the efficiency and accuracy of plate fixation for fractures.

*Address correspondence to this author at the Key Laboratory of High Efficiency and Clean Mechanical Manufacture (Ministry of Education), School of Mechanical Engineering, Shandong University, Jinan 250061, China;
Tel: +86-0531-88392850; E-mail: zhangqh@sdu.edu.cn

E-ISSN: 2409-9694/23

The following are the details of the research in the subsequent chapters of this study.

Firstly, the finite element model of cortical bone drilling is established based on ABAQUS, and the maximum torque and axial force of drilling are determined based on the simulation results, which provides a basis for the selection of electric batches. Then, the mechanical structure of the steel plate fixation device was designed by using SOLIDWORKS and introduced its working principle and workflow. And then, based on the virtual prototype technology, the kinematic and dynamics simulation using ADAMS is performed to verify the working principle of the device and the feasibility of the structure. In addition, the modal analysis of the device is performed using ABAQUS, and the static analysis of the components with large forces is carried out to prove that the structure can meet the requirements of use. Finally, the study is summarized and gives the outlook of the subsequent work.

2. ABAQUS-BASED FINITE ELEMENT MODEL FOR CORTICAL BONE DRILLING

To design a robot-assisted lower limb fracture plate fixation device, the first step is to select a suitable bone drilling tool and to calibrate the strength of the drilling rod. In this section, a finite element model of cortical bone drilling is established based on ABAQUS to obtain the torque and axial force when drilling the cortical bone.

In this section, a standard medical twist drill was used for the drilling study of cortical bone, and the structural parameters of the drill were provided by the manufacturer as follows: top angle 2Φ = 118° and helix angle β = 30°. To reduce the number of meshes and calculation time, the twist drill shape was simplified by ignoring the neck and tail of the twist drill and only creating a 3D model of the twist drill bit in SOLIDWORKS. Ignoring the irregular shape of the cortical bone, only consider the cortical bone in contact with the drilling part of the drill bit. The cortical bone can be modeled as a rectangular body with a shape size of 8mm×8mm×4mm, and the drill bit and cortical bone are assembled and saved as x_t format and imported into the finite element software ABAQUS6.14, as shown in Figure **1**.

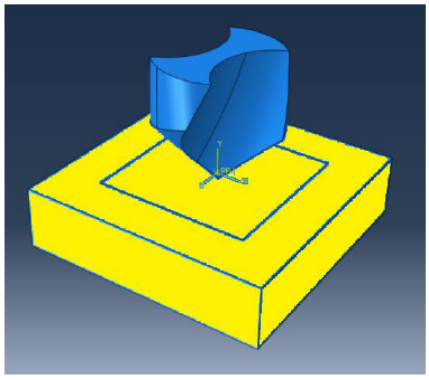

Figure 1: Cortical bone drilling geometry model.

The material of the twist drill is stainless steel, and the cortical bone data below use the material parameters of the bovine femur measured by K. Fu [10]. The twist drill and cortical bone parameters are shown in Table **1**.

Table 1: Parameters of Twist Drill and Cortical Bone Material

Parameter	Twist Drill	Cortical Bone
Density （kg/m3）	7840	1700
Young's modulus （GPa）	210	13.8
Specific heat （J/kg·°C）	490	1260
Thermal conductivity （W/m·°C）	4.5×10^{-4}	2.49×10^{-2}
Poisson ratio	0.3	0.35

The Johnson-Cook intrinsic model is used in 3D cutting simulation experiments because it reflects not only the strain-strain rate dependence of the material but also the temperature-softening effect of the material [11], so this model is chosen as the intrinsic model of cortical bone in this study. The expression for the Johnson-Cook model is as follows:

$$\bar{\sigma} = (A + B\varepsilon^{n})\left(1 + C\ln\frac{\dot{\varepsilon}}{\dot{\varepsilon}_{0}}\right)\left[1 - \left(\frac{T - T_{r}}{T_{m} - T_{r}}\right)^{m}\right] \quad (1)$$

In the formula,

A ——Yield stress of the material（MPa);

B ——Work-hardening modulus (MPa);

C ——Strain rate sensitivity factor;

n ——Hardening factor;

m ——Thermal softening coefficient of the material.

A, B, C, n, and m are constants determined by the properties of the material itself, ε is the strain, ε^{n} is the equivalent plastic strain, ε_{0} is the reference strain, T_m

Table 2: Parameters of the Johnson-Cook Model for Cortical Bone

A（MPa）	B（MPa）	n	C	m	T_m（°C）
50	101	0.08	0.03	1.03	1400

is the melting point of the material (℃), and T_r is the ambient temperature (℃), which is usually expressed as the room temperature.

The first term of this constitutive equation represents the quasi-static properties when the temperature of the material is equal to room temperature and the strain rate is equal to the reference strain rate, which can be obtained by automatic ballast experiments; The second term indicates the strain rate reinforcement effect of the material, which can be measured by the Hopkinson pressure bar test apparatus; The third term is the thermal softening effect of the material. The parameters of the Johnson-Cook model for cortical bone are shown in Table **2**.

In the ABAQUS/Explicit module, the mesh division has a significant impact on the calculation results of finite element simulation. To ensure the accuracy of the finite element analysis process, the mesh type and mesh density should be set reasonably when meshing the cortical bone and the drill bit. The cortical bone involved in drilling is mainly the middle part, and the mesh is refined for this area, while the surrounding area has less influence on the simulation results, and a relatively sparse mesh can be used. The mesh size of the middle part is controlled within 0.1mm, and the mesh size of the other areas of the cortical bone and the drill bit is controlled within 1mm. The mesh of the cortical bone is divided by the solid three-dimensional four-node tetrahedral cell (C3D4), and the number of the divided mesh is 64300; the mesh of the drill bit is divided by the solid three-dimensional eight-node hexahedral cell (C3D8), and the divided mesh is 9917. The quality of all the meshes divided by the test is qualified, and the mesh division is shown in Figure **2**.

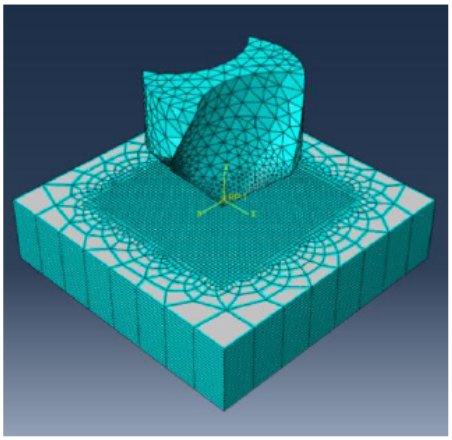

Figure 2: Cortical bone drilling meshing.

Based on the actual drilling situation, define the boundary conditions and initial conditions. The four sides of the cortical bone model are completely fixed to restrict its motion; the feed speed and rotation speed of the drill are set in the LOAD module of ABAQUS, and the other four degrees of freedom are restricted. The boundary conditions and initial conditions are set as shown in Figure **3**.

According to the above, the cortical bone drilling process was simulated by using ABAQUS to record the

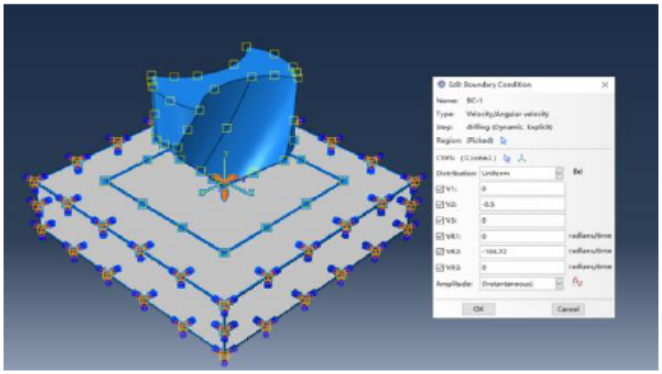

Figure 3: Boundary conditions and initial conditions.

Table 3: Torque and Axial Force Simulation Results

Number	Feeding speed (mm/min)	RPM (r/min)	Torque (N·m)	Axial force (N)
1	20	800	0.0279	28.24
2	20	1000	0.0251	26.92
3	20	1200	0.0229	25.94
4	30	800	0.0352	35.71
5	30	1000	0.0315	34.15
6	30	1200	0.0288	32.85
7	40	800	0.0414	42.26
8	40	1000	0.0378	40.37
9	40	1200	0.0341	38.93

changes in torque and axial force. Based on the clinical data of Shandong Provincial Hospital of Traditional Chinese Medicine, the feed speed was selected at three levels of 20 mm/min, 30 mm/min, and 40 mm/min, and the RPM was selected at three levels of 800 r/min, 1000 r/min, and 1200 r/min, and the simulation results are shown in Table **3**.

According to the simulation results, the maximum drilling axial force in the range of feed rate 20mm/min-40mm/min and speed 800r/min-1200r/min is 42.26N and the maximum torque is 0.0414N-m, this provides a reference basis for the torque and axial force that the device needs to provide.

3. STRUCTURAL DESIGN OF THE STEEL PLATE INTERNAL FIXING DEVICE

Robot-assisted automatic plate fixation device for lower limb fracture is shown in Figure **4**, which mainly consists of two major parts: robot system and plate fixation device. The robot arm has six degrees of freedom and the repeat positioning accuracy is ±0.02mm, which can accurately move the nail placement device to the appropriate nail placement position. The fixing device mainly includes the driving mechanism, drilling mechanism, nail supply mechanism, nail placement mechanism, guide sleeve, and outer shell, as shown in Figure **5**. The device can realize the function of drilling and nail placement at the same time, and the speed and feed rate of drilling can be adjusted on demand, which has the advantages of high drilling efficiency, accurate nail placement, and high automation. The following is a brief description of the main structure.

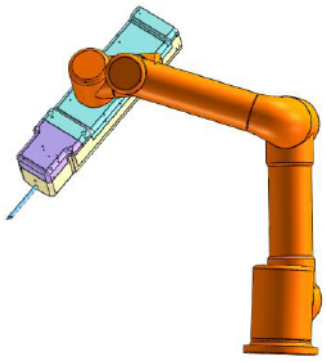

Figure 4: Schematic diagram of steel plate internal fixation device installed at the end of mechanical arm.

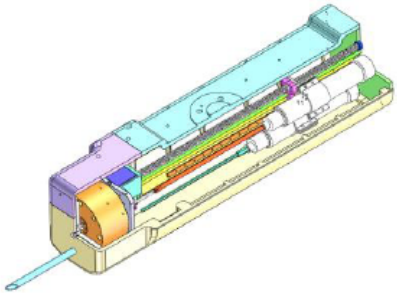

Figure 5: Structural drawing of steel plate internal fixation device.

3.1. Drill Mechanism

The drilling mechanism is one of the core components of the plate internal fixation device, and its main function is to process the screw pre-holes in the hard bone tissue. The drilling mechanism mainly consists of a drilling electric batch, a drilling rod, a stainless steel twist drill bit, a guide, a slider, and an electric batch clamping plate, the specific structure of which is shown in Figure **6**.

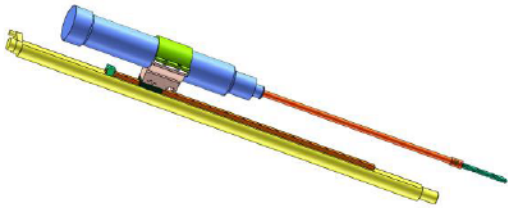

Figure 6: Drilling mechanism.

The electric drill provides the main power for bone drilling and transmits the power to the drill bit through the drill bar to complete the drilling of cortical bone. The drill bar end is connected to the drill bit-by-side fastening, which is simple and convenient to install. When the drill bit is installed, it needs to be installed to the positioning pin position and then fastened with screws to prevent relative sliding or axial jumping of the drill bit and the drill rod when drilling the bone. There are two main parameters of the bone drilling electric drill, power and torque. According to the bone drilling parameters commonly used in clinical practice, the speed of the electric batch should be no less than 2000r/min, and the simulation results in the second section, the maximum drilling torque is 0.0414N-m when the drill diameter is 4mm, so the maximum torque of the electric batch can be calculated by equation 2.

$$M \geq S_d M_{Dilling} \tag{2}$$

The S_a is the safety factor, this chapter takes the value of 2, and the torque of the electric batch can be calculated to be greater than 0.09N-m, therefore, the power of the electric batch can be calculated by the formula 3-2.

$$P = \frac{N \cdot M}{9550} \tag{3}$$

The power of the electric batch is P (W); N is the speed of the electric batch, M is the maximum torque of the electric batch, and the power of the electric batch should be not less than 18.9W.

The drilling electric batch is connected to the slider through the electric batch clamping plate, the slider is mounted on the guide rail, and the guide rail is connected to the arbor by screws. The upper and lower electric batch clamping plate fixes the electric batch by hexagonal bolt clamping, and the four threaded holes at the top are connected to the slider, the lower electric batch clamping plate has a groove with the electric batch pushing block, and the pushing block is connected to the screw nut by bolt, when the tab at the top of the pushing block is in the groove, the screw nut can drive the drilling electric batch to move along the guide rail, when the tab at the top of the pushing block is not in the groove, the screw nut will not drive the drilling electric batch to move.

3.2. Nailing Mechanism

Nail placement is one of the most essential steps of plate fixation surgery, which directly affects plate fixation and postoperative recovery. The main function of the nail placement mechanism is to screw the internal fixation screws into the screw pre-holes. The nail placement mechanism consists of a nailer, a screwdriver, a guide, a slider, and a nailer clamping plate, and its structure is similar to the drilling mechanism, as shown in Figure **7**.

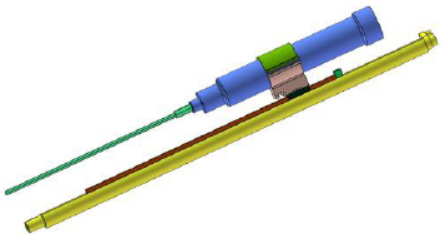

Figure 7: Nailing mechanism.

The screws placed in this design are self-tapping screws, eliminating the need to design a tapping device and making the device lighter while reducing operating time.

3.3. Nail Supply Mechanism

The nail supply mechanism provides the internal fixing screw for the device, which mainly consists of a turntable, paddle, paddle top lever, bearing, front stopper, rear stopper, spring plunger, top pin, and turntable shaft, the mechanism shown in Figure **8**.

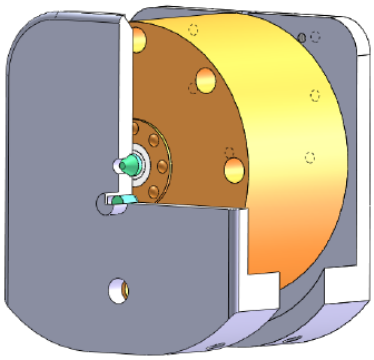

Figure 8: Nail supply mechanism.

There are eight evenly spaced screw holes on the turntable for the drill bit to extend and accommodate the screws, and several spherical grooves on the front

surface of the turntable to cooperate with the top pin to realize the positioning of the turntable. At the bottom of the top pin, there is a spring installed, and the head of the top pin fits closely with the spherical grooves on the front surface of the turntable under the action of the spring, which prevents the turntable from rotating randomly. There are several shaped grooves evenly distributed on the rear surface of the turntable, and the shaped grooves are divided into a flat bottom groove part and a beveled groove part, which cooperate with the paddle top lever to realize the one-way rotation of the turntable, as shown in Figure **9**.

When the paddle is rotated in the counterclockwise direction as shown in Figure **9**, the paddle top lever can slide out along the beveled groove on the rear end face of the turntable, and the resulting paddle force is less than the resistance provided by the top pin, and the turntable does not rotate; When the paddle rotates clockwise, the paddle top lever cooperates with the flat bottom groove part on the rear end face of the turntable, and the resulting paddle force is greater than the resistance provided by the top pin, and the turntable rotates to achieve accurate positioning to the next hole with each paddle movement. The spring plunger fits into the beveled groove on the baffle plate for easy installation and removal of the turntable. At installation, the inclined groove compresses the spring plunger, and the turntable can be installed smoothly to the top pin to achieve the positioning of the turntable, at this time the spring plunger returns to its original length and fixes the turntable arbor. For disassembly, simply compress the spring-loaded plunger and pull out the turntable upwards. The nail supply mechanism performs a ratchet-like function, providing a switch of screw-holding holes to supply the required screws to the screw screw-in mechanism.

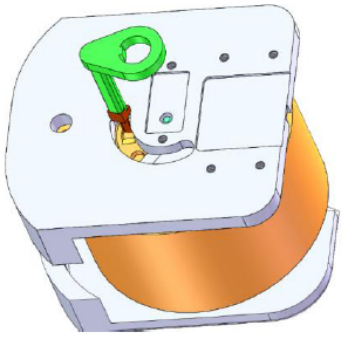

Figure 9: Turntable one-way toggle schematic.

3.4. Working State Transition Mechanism

As shown in Figure **10**, the servo drives the arbor to rotate to achieve the conversion of drilling and nailing positions. When the servo turns to the drilling position, the groove on the top of the clamping plate of the drilling electric batch is just stuck to the tab on the top of the electric batch push block, the push block and the screw nut are fastened by bolts to drive the drilling electric batch to finish the drilling; when the servo turns to the nailing position, the groove on the top of the clamping plate of the nailing electric batch is just stuck to the tab on the top of the electric batch push block, and it can be pushed forward by the electric batch push block to place the inner fixing screw into the pre-holes.

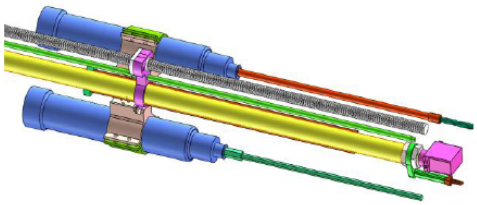

Figure 10: Workstation conversion schematic.

3.5. Workflow of the Device

The device is controlled by a stepper motor and servo to achieve the function of drilling first and then nail placement, the specific process is shown in Figure **11**.

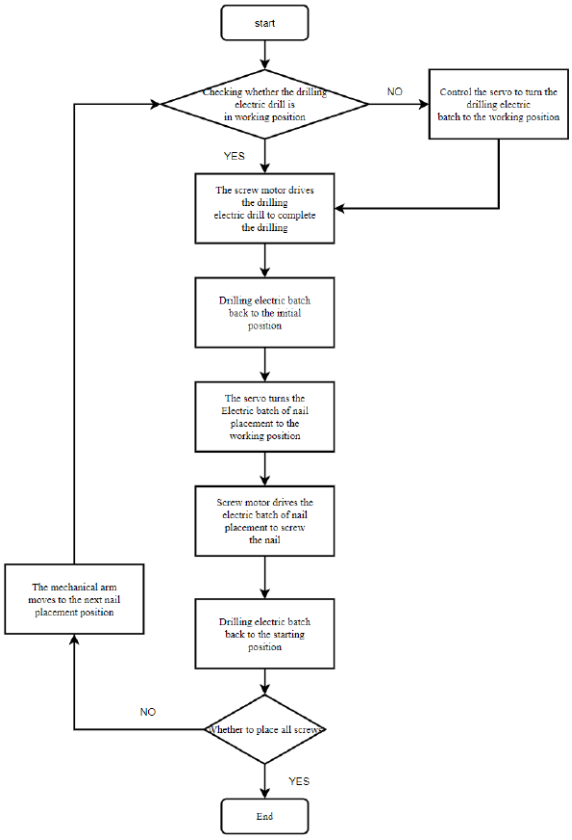

Figure 11: Device workflow diagram.

4. SIMULATION ANALYSIS OF THE PLATE INTERNAL FIXATION DEVICE

In this chapter, to verify the working principle of the device and whether the design is reasonable, kinematic simulation and dynamics simulation are carried out using virtual prototype technology, and whether the selected rudder load capacity meets the working requirements are verified.

4.1. Kinematics and Dynamics Simulation

The internal fixtures created in Section 3 were imported into ADAMS for simulation. To improve the simulation efficiency, the models of mechanical screws, bearings, and upper housing that do not affect the motion relationship are removed. The imported model of the internal fixation device is shown in Figure **12**.

The parts imported into the ADAMS/View simulation model of the internal fixing device are subjected to Boolean operations, and the parts with consistent motion and no relative motion are combined to simplify the model. Apply fixation subsets to the support parts and the housing to fix them to the ground. The kinematic subs and drives are added to the parts with a motion to limit the relative motion between the parts. The kinematic subs used are mainly low, and the low sub-module mainly includes rotating subs, spiral subs, and moving subs. The kinematic subs and drives are added as shown in Table **4**.

The movement of the electric screwdriver along the guide on the arbor is achieved by a push block fixed to the nut, so it is necessary to create a contact between the push block and the connector holding the electric screwdriver to achieve force transmission. Similarly, the unidirectional rotation of the turntable is achieved by the paddle with the backstop and the groove on the turntable, so it is necessary to create contact between the paddle top bar and the turntable and between the paddle top bar and the backstop. In addition, torsional spring forces should be set in the ADAMS model between the paddle and the paddle top bar, and spring forces between the top pin and the front baffle, to more realistically simulate the load on the device during actual operation.

In the model imported into ADAMS with the nail placement electric screwdriver in the working position,

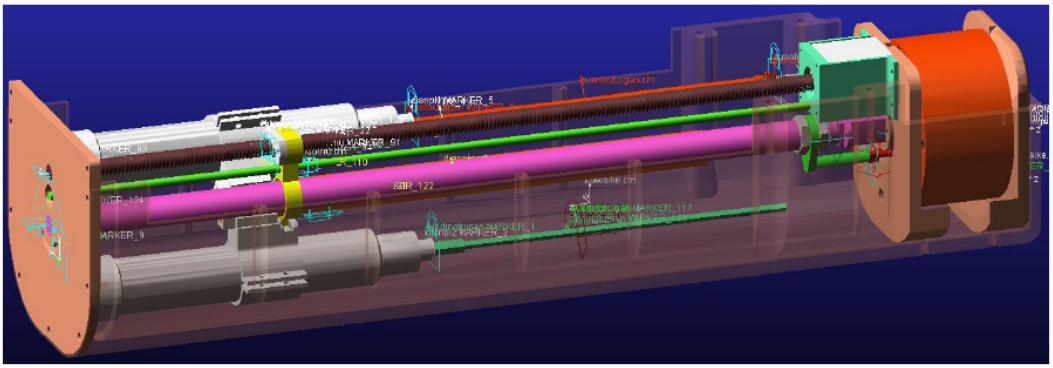

Figure 12: ADAMS simulation model of the internal fixation device.

Table 4: Motion Sub and Drive Additions

Motion Components	Type of sports sub	Drive Type
Screws, nuts	Spiral sub, moving sub	None
Screws, motors	Rotating sub	Rotary drive MOTION1
Paddle, paddle top lever	Rotating sub	None
Electric Screwdriver, Guide	Mobile Vice	None
Turntable top pin, front stopper	Mobile Vice	None
Arbor, Servo	Rotating sub	Rotary drive MOTION2
Turntable, turntable shaft	Rotating sub	None

the control timing is designed as shown in Table **5** for the device to achieve drilling first and then nail placement.

Table 5: Control Timing Table

Serial number	Time(s)	Action
1	0-2	Arbor rotates 120°, drilling motor reaches the working position
2	2-71.9	The drill bit is fed forward to complete the drilling
3	71.9-82.9	Drilling the electric screwdriver back, return to the initial position
4	82.9-84.9	The arbor is reversed 120°, and the nailer reaches the working position.
5	84.9-97.575	Screwdriver feeds forward to complete nail placement
6	97.575-108.175	Set the nail batch back and return to the initial position

After step 6 is completed, return to step 1 and run the sequence again to screw in the next cortical bone screw.

This section uses the step function to control the rotational sub-speed of the screw and servo, and the obtained speed curve will be plotted as shown in Figure **13**, where the vertical coordinate unit is radians per second and the horizontal coordinate unit is seconds.

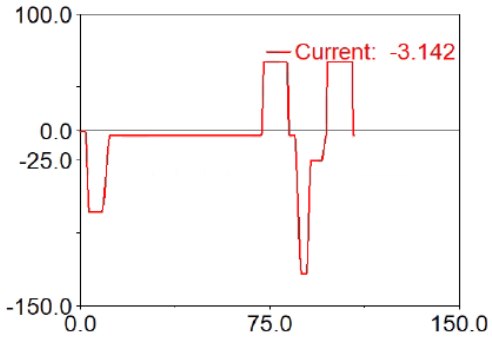

Figure 13: Rotational speed curve of screw rotating sub.

This chapter uses the step function to control the rotational speed of this rotational sub, and the speed curve obtained is shown in Figure **14**.

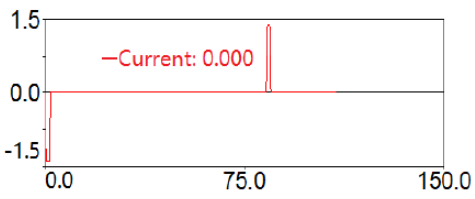

Figure 14: Servo speed curve.

This paper uses an interactive simulation with the duration set to 108.5 seconds and the step count set to 10,000 steps. After the simulation, ADAMS can provide the motion curve and load curve of each part, and export the data in Origin for processing.

The screw nut motion curve and load curve are shown in Figure **15**. Since the simulation model in this chapter does not set the friction force, the screw nut load force is 0 when the screw does uniform rotation, and the screw nut is loaded when the screw does uniform acceleration or uniform deceleration motion, which matches the nut load curve in Figure **15**.

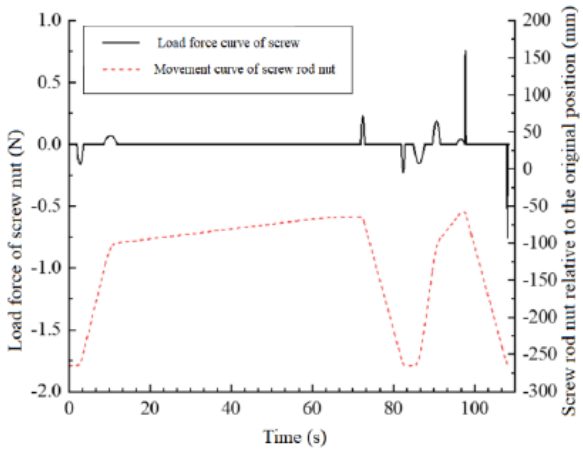

Figure 15: Motion curve and load curve of the screw nut.

The movement curve of the drilling electric screwdriver is shown in Figure **16**, comparing the movement curve of the drilling electric screwdriver with the speed curve of the servo, we can see that when the servo rotates, the X coordinate and Y coordinate of the core of the drilling electric screwdriver change, but the Z coordinate remains unchanged, at this time, the drilling electric screwdriver rotates around the core axis in the X-Y plane; comparing the movement curve of the drilling electric screwdriver with the Z coordinate curve of the center of the screw nut, we can see that the Z coordinate of the core of the drilling electric screwdriver and the Z coordinate of the center of the screw nut are the same in the 2s-82.9s. The trend of the Z coordinate curve of the center and the Z coordinate curve of the screw nut is the same, and the X and Y coordinates of the center do not change, at this time, the drilling electric screwdriver does the feeding and retracting movement along the Z direction. The movement law of the drill batch is in full compliance with the working requirements and expected assumptions, and the working principle of the device is feasible.

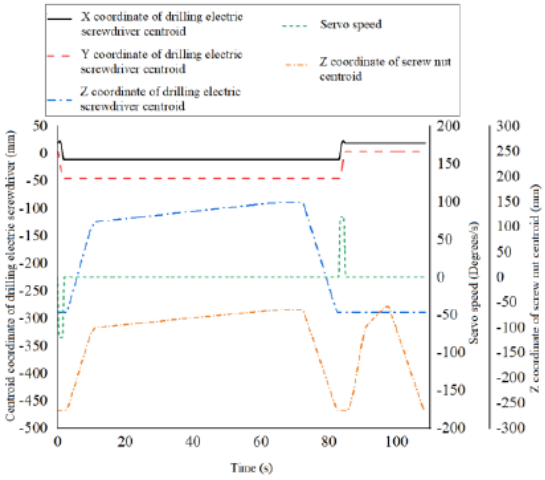

Figure 16: Drilling electric screwdriver movement curve.

The movement curve of the nail batch is shown in Figure **17**, comparing the movement curve of the nail batch with the speed curve of the servo, it can be seen that the X coordinate and Y coordinate of the nail batch center of mass change when the servo rotates, and the Z coordinate remains unchanged, at this time the nail batch rotates around the core axis in the X-Y plane; comparing the movement curve of the nail batch with the Z coordinate curve of the center of mass of the screw nut, it can be seen that the Z coordinate of the nail batch center of mass changes from 84.9s to 108.175s, and the Z coordinate of the center of mass of the nail batch does not change in the direction of the Z axis. The trend of the Z-coordinate of the nailer and Z-coordinate of the screw nut is the same, and the X and Y coordinates of the nailer do not change, at this time the nailer does the feeding and retracting movement along the Z-axis. The movement law of the nailer is fully in line with the working requirements and expected assumptions, and the working principle of the device is feasible.

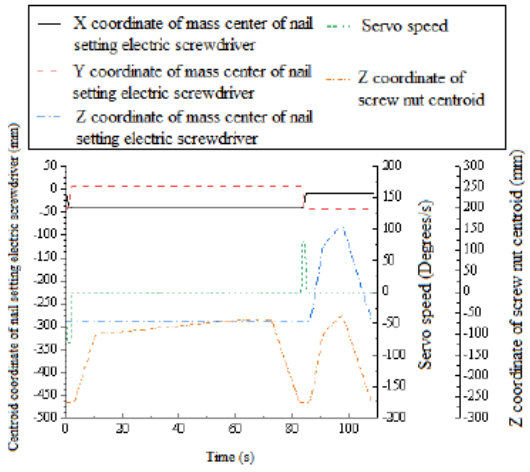

Figure 17: Movement curve of nail placement electric screwdriver.

The relationship between rudder torque and rotational speed is shown in Figure **18**, in 0-2s and 82.9-84.9s rudder rotation, the rudder output torque drives the mandrel rotation, in figure 82.9-84.9s rudder torque is greater than 0-2s rudder torque, this is caused by the one-way rotation of the turntable, in 0-2s rudder rotation the paddle top lever does not make the turntable rotate, 82.9-84.9s rudder rotation But due to the existence of the turntable top pin, the rudder needs to overcome the resistance of the turntable top pin to the turntable, so the 82.9-84.9s rudder torque is greater than the 0-2s rudder torque. From Figure **18**, we can see that the maximum rudder torque is 150N-mm, which does not exceed the maximum torque of the selected rudder, so the rudder meets the requirements of use.

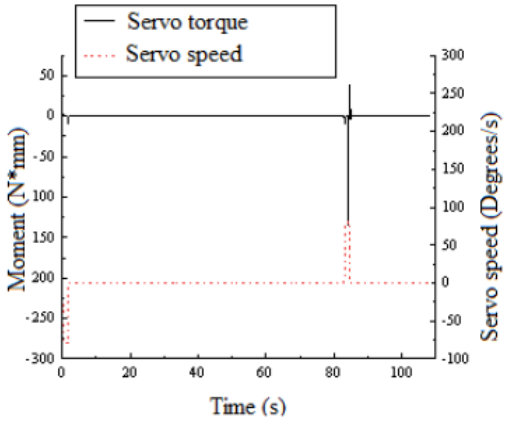

Figure 18: Servo torque versus speed.

4.2. Modal Analysis

Modal analysis of the mechanical system can obtain its inherent frequency and modal vibration pattern, and then avoid resonance of the mechanical structure [12], this section uses ABAQUS to perform modal analysis of the designed fixture, and the material parameters of each component are shown in Table **6**. The positive

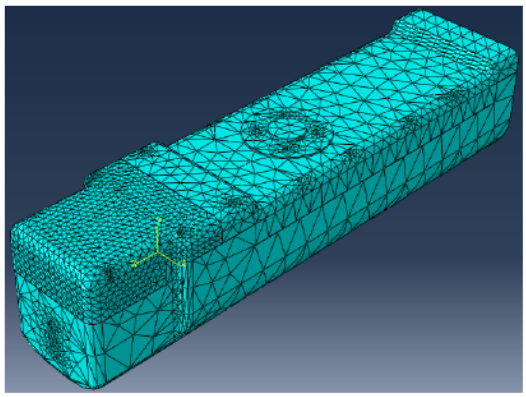

Figure 19: Internal fixation device mesh division.

tetrahedral structure C3D10 is selected to perform uniform meshing of the model, and Figure **19** shows the model after meshing. Finally, the constraints are added, the boundary conditions of the system are set, and the calculation of the modal analysis is carried out.

Table 6: Table of Material Parameters of Each Component

Parts	Materials	Density	Modulus of elasticity	Poisson's ratio
Screws, guide shafts, arbors, electric screwdriver push blocks	45 gauge steel	7.9	210	0.275
Paddle, baffle, housing, turntable	Aluminum alloy	2.68	70	0.33
Guide rails, sliders, drill bits, drill rods, screwdrivers	Stainless Steel	8	190	0.29
Screw nuts	Copper Alloy	7.4	110	0.3

The higher-order modes are often neglected due to their lower energy share and smaller impact on the vibration of the structure [13]. Therefore, the first six modal frequencies are selected for analysis in this paper. To better understand the vibration of each mode, the deformation is enlarged by 47.87 times, the intrinsic frequency and mode vibration pattern are shown in Table **7**, and the mode cloud diagram is shown in Figure **20**.

Table 7: Table of the First Six Orders of Inherent Frequency and Modal Vibration Pattern

Modal Order	Inherent freqçuency (Hz)	Modal Vibration Pattern
First order	78.727	The reciprocating movement of the drill pipe along the Y-axis
Second order	78.799	The reciprocating movement of the drill pipe along the X-axis
Third Order	93.298	The reciprocating movement of the screwdriver along the X-axis
Fourth Order	93.671	The reciprocating movement of the screwdriver along the Y-axis
Fifth Order	108.48	The whole body is centered on the fixed point of the flange and oscillates reciprocally around the X-axis
Sixth Order	151.86	Arbor, drill rod, and screwdriver swing left and right along the X-axis

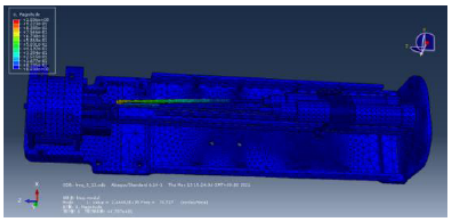

(**a**) First-order mode

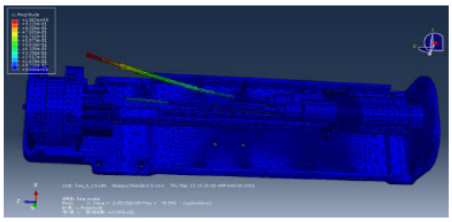

(**b**) Second-order mode

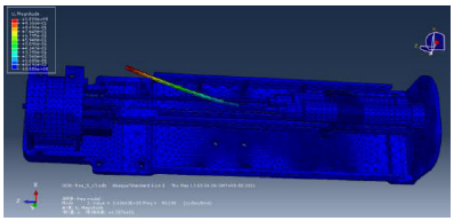

(**c**) Third-order mode

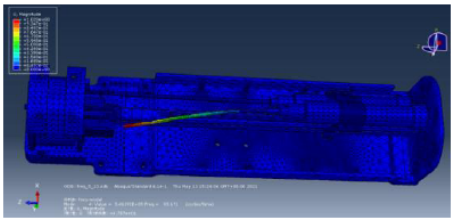

(**d**) Fourth-order mode

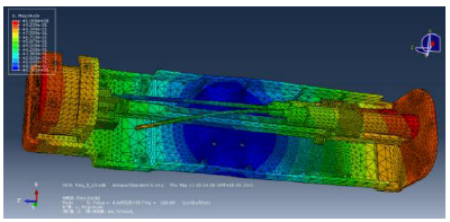

(**e**) Fifth-order mode

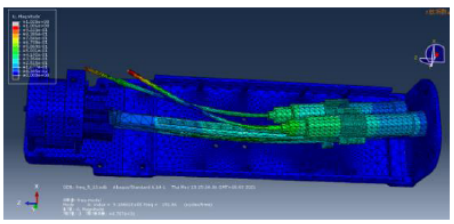

(**f**) Sixth-order mode

Figure 20: Modal cloud diagram of the internal fixation device.

The mechanical structure designed in this paper has a maximum motor speed of 1200 r/min, *i.e.*, the working frequency is 20 Hz. Comparing the first six orders of modal frequencies obtained from the modal analysis, it can be seen that the inherent frequency of the mechanical structure designed in this paper completely avoids the working frequency of the motor and the mandrel, *i.e.*, the mechanical structure designed in this paper is not easy to resonate during normal operation and has good dynamic performance, which verifies the correctness of the structure.

4.3. Static Analysis of the Key Components

When the structure is designed, the static analysis should be performed to determine whether the structure has sufficient strength and stiffness under the premise of meeting the functional requirements. The electric screwdriver push block is the main force member to push the electric screwdriver to do the feeding movement, the drill push rod and screwdriver are the main force member when drilling and nail placement, they are deformed under the action of external load when the deformation is too large or the stress is too high, it will not be able to meet the needs of normal work, so it is necessary to conduct static analysis on these key parts to check their strength.

4.3.1. Static Analysis of the Electric Screwdriver Push Block

The three-dimensional model of the electric screwdriver push block is saved as x_t format and imported into ABAQUS, and the ABAQUS simulation model is established for solving, and the calculation results are shown in Figures **21** and **22**.

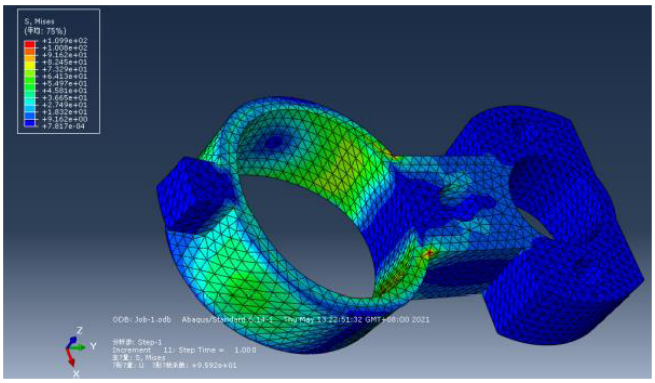

Figure 21: Electric screwdriver push block stress cloud.

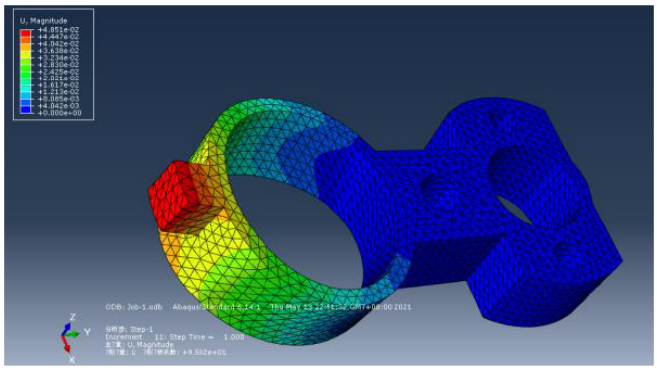

Figure 22: Electric screwdriver push block displacement cloud.

As can be seen from Figure **21**, the maximum stress occurs at the lower part of the circle where the shape is abruptly changed, and the maximum stress is 109.94 MPa. The material of the electric screwdriver push block is No. 45 steel, and the yield strength is 355 MPa, which meets the strength requirement. As can be seen from Figure **22**, the maximum displacement occurs at the top of the head bump with a maximum strain of 0.049mm, and the deformation is small and does not adversely affect the feeding motion.

4.3.2. Flexural Analysis of the Drill Pipe

The drilling rod and screwdriver are cantilever beams with one end fixed and one end under pressure, which will produce the problem of destabilization of the compression rod when the stress is too high and then lose the load-bearing capacity. To verify the structural stability of the drilling rod and screwdriver, it is necessary to perform a flexural analysis.

In this paper, the classical static buckling analysis method is used to obtain the critical buckling load, which is used to represent the upper limit of the critical buckling value of the structure. C3D10 cells are used to delineate the mesh of the drill pipe model with a mesh size of 1mm, and the drill pipe is fixed at one end and restricted at the other end to all degrees of freedom except axial and rotation along the axis, while lateral axis rotation is allowed and radial displacement of the end nodes is not restricted. The eigenvalue buckling analysis requires activation of pre-stress effects, so a surface load of 1 N is applied to the drill pipe model. Five eigenvalues of the drill pipe were obtained, and the eigenvalues are shown in Table **8** and the cloud diagram is shown in Figure **23**.

Table 8: Characteristic Values of Drill Pipe Flexure Analysis

Number of steps	First order	Second order	Third Order	Fourth order	Fifth Order
Eigenvalue	439.69	440.15	3960.1	3962.8	11009

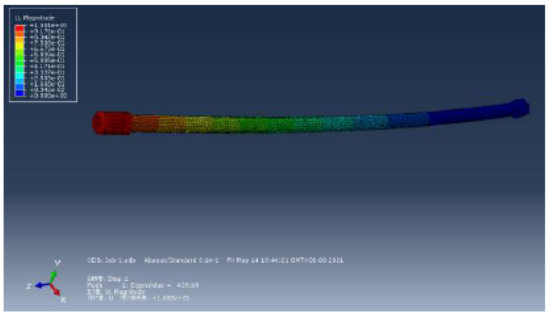

(**a**) First order

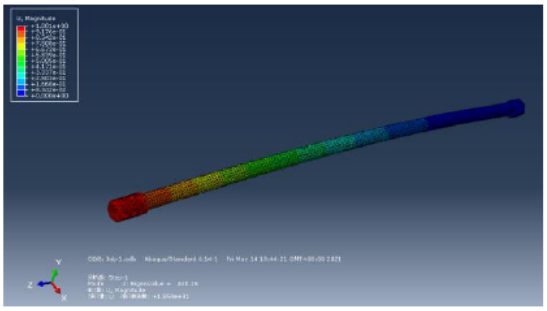

(**b**) Second order

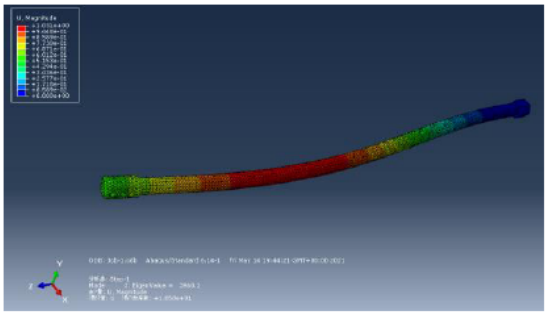

(**c**) Third order

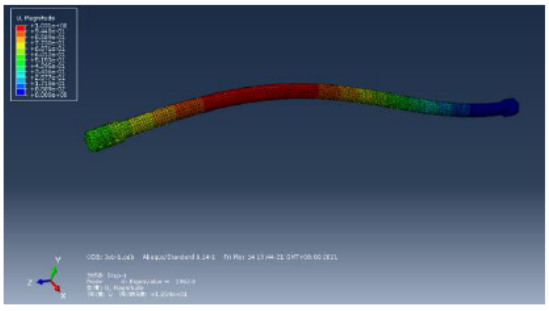

(**d**) Fourth order

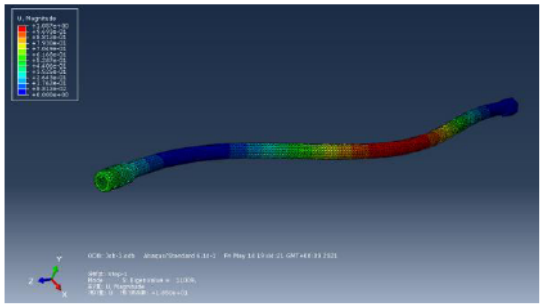

(**e**) Fifth order

Figure 23: Drill pipe flexion cloud.

Eigenvalue buckling analysis is a linear solution method, which is more efficient to calculate, but ignoring the nonlinear behavior also leads to relatively conservative calculation results. In practical applications, a safety factor of 3 to 5 times can be set to solve. The load set in this paper is 1N, and the first-order critical buckling load is 439.69N, which is equal to the product of the eigenvalue and the applied load. The maximum axial pressure on the drill pipe is 42.26N, and the calculated safety factor is 10.4, so the designed drill pipe structure is more stable.

The screwdriver is made of the same material as the drill pipe, with a smaller length than the drill pipe, better rigidity, and less force than the drill pipe, so it has better stability, and no more flexural analysis of the screwdriver is performed.

5. CONCLUSION

In this paper, a screw placement device for fixing fracture plates is designed and analyzed kinematically, dynamically, modally, and statically. The device can be used with a robotic arm to improve the continuity and accuracy of screw insertion. The kinematic and kinetic simulations of the device were carried out using virtual prototype technology, the kinematic curves of each component of the device were obtained, and the workflow diagrams were compared to show that the device achieves the expected working concept, and the kinetic simulations verified that the selected servo can meet the working requirements. The modal analysis of the whole device was carried out using FEA software, and the modal frequencies and modal vibration

patterns of the first six orders were analyzed to verify that the device is not susceptible to resonance during normal operation. The key components of the device were checked for static strength and their structural stability was verified.

The screw placement device proposed in this paper can achieve the expected function and can work stably, but there is still a lack of lightweight design, and the research content of this paper only involves the hardware part of the device, still need to develop the corresponding control system.

DECLARATION OF COMPETING INTEREST

The authors declare no conflict of interest.

ACKNOWLEDGMENTS

This work was supported by the National Natural Science Foundation of China (52075301), the National Key R&D Program of China (2019YFC0119200), the Key R&D Program of Shandong Province (2019GHZ002), and the Natural Science Foundation of Shandong Province (ZR2019MEE017).

REFERENCE

[1] Leunig M, Hertel R, Siebenrock K A, *et al*. The evolution of indirect reduction techniques for the treatment of fractures. Clinical Orthopaedics & Related Research, 2000; 375: 7. https://doi.org/10.1097/00003086-200006000-00003

[2] Bouazza-Marouf K, Browbank I, Hewit J R. Robotic-assisted internal fixation of femoral fractures. Proceedings of the Institution of Mechanical Engineers Part H Journal of Engineering in Medicine, 1995; 209(1): 51-58. https://doi.org/10.1243/PIME_PROC_1995_209_316_02

[3] Browbank I, Bouazza-Marouf K, Schnabler J. Robotic-assisted internal fixation of hip fractures: a fluoroscopy-based intraoperative registration technique. Proc Inst Mech Eng H, 2000; 214(2): 165-179. https://doi.org/10.1243/0954411001535336

[4] Füchtmeier B, Egersdoerfer S, Mai R, *et al*. Reduction of femoral shaft fractures in vitro by a new developed reduction robot system 'RepoRobo'. Injury-International Journal of the Care of the Injured, 2004; 35(1-supp-S): 113-119. https://doi.org/10.1016/j.injury.2004.05.019

[5] Maeda Y, Sugano N, Saito M, *et al*. Robot-assisted femoral fracture reduction: a preliminary study in patients and healthy volunteers. Computer Aided Surgery, 2008; 13(3): 148-156. https://doi.org/10.3109/10929080802031038

[6] Tian W, Han X, Liu B, *et al*. A Robot-Assisted Surgical System Using a Force-Image Control Method for Pedicle Screw Insertion. PLoS One, 2014; 9(1). https://doi.org/10.1371/journal.pone.0086346

[7] Hu L, Luan S, Wang M Y, *et al*. A biplanar robot navigation system for the distal locking of intramedullary nails. Int J Med Robotics Comput Assist Surg, 2010; 6(1): 61-65. https://doi.org/10.1002/rcs.289

[8] Keric N, Doenitz C, Haj A, *et al*. Evaluation of robot-guided minimally invasive implantation of 2067 pedicle screws. Neurosurg Focus, 2017; 42(5): E11. https://doi.org/10.3171/2017.2.FOCUS16552

[9] Chenin L, Peltier J, Lefranc M. Minimally invasive transforaminal lumbar interbody fusion with the ROSA (TM) Spine robot and intraoperative flat- panel CT guidance. Acta Neurochir (Wien), 2016; 158(6): 1125-1128. https://doi.org/10.1007/s00701-016-2799-z

[10] K.K. Fu Jiang. Research on drilling temperature and drilling quality of tooth groove bone. Shandong University, 2018.

[11] A. Haglund, On Friction Modeling in Orthogonal Machining: An Arbitrary Lagrangian-Eulerian Finite Element Model. 200545(5).

[12] L. Shao, *et al*. "Experimental and numerical modal analysis of wall tubes in the coal-fired boiler or radiant syngas cooler," Canadian Journal of Chemical Engineering, 2022; 100(10): 2918-2927. https://doi.org/10.1002/cjce.24294

[13] A. Amirian, S. E. M. Torshizi and S. H. Dibajian, "Experimental and numerical investigation of the effect of microstructural changes on the vibrational characteristics of ck35 steel," Proceedings of the Institution of Mechanical Engineers. part C, Journal of Mechanical Engineering Science, 2022; 236(3): 1363-1376. https://doi.org/10.1177/09544062211020783

Received on 20-12-2022 Accepted on 18-01-2023 Published on 24-01-2023

DOI: https://doi.org/10.31875/2409-9694.2023.10.01